

LETTERS

SAGA interacting factors confine sub-diffusion of transcribed genes to the nuclear envelope

Ghislain G. Cabal^{1*}, Auguste Genovesio^{2*}†, Susana Rodriguez-Navarro^{4†}, Christophe Zimmer², Olivier Gadal¹, Annick Lesne⁵, Henri Buc³, Frank Feuerbach-Fournier¹, Jean-Christophe Olivo-Marin², Eduard C. Hurt⁴ & Ulf Nehrbass⁶

Changes in the transcriptional state of genes have been correlated with their repositioning within the nuclear space¹. Tethering reporter genes to the nuclear envelope alone can impose repression² and recent reports have shown that, after activation, certain genes can also be found closer to the nuclear periphery^{3–6}. The molecular mechanisms underlying these phenomena have remained elusive. Here, with the use of dynamic three-dimensional tracking of a single locus in live yeast (*Saccharomyces cerevisiae*) cells, we show that the activation of *GAL* genes (*GAL7*, *GAL10* and *GAL1*) leads to a confinement in dynamic motility. We demonstrate that the *GAL* locus is subject to sub-diffusive movement, which after activation can become constrained to a two-dimensional sliding motion along the nuclear envelope. RNA-fluorescence *in situ* hybridization analysis after activation reveals a higher transcriptional activity for the peripherally constrained *GAL* genes than for loci remaining intranuclear. This confinement was mediated by Sus1 and Ada2, members of the SAGA histone acetyltransferase complex, and Sac3, a messenger RNA export factor, physically linking the activated *GAL* genes to the nuclear-pore-complex component Nup1. Deleting *ADA2* or *NUPI* abrogates perinuclear *GAL* confinement without affecting *GAL1* transcription. Accordingly, transcriptional activation is necessary but not sufficient for the confinement of *GAL* genes at the nuclear periphery. The observed real-time dynamic mooring of active *GAL* genes to the inner side of the nuclear pore complex is in accordance with the 'gene gating' hypothesis⁷.

To analyse directly the possibility of activation-dependent changes in the dynamic motility of genes, and to gain a better understanding of activation-dependent nuclear repositioning at a molecular level, we developed a dedicated imaging approach (see Methods). In brief, by combining real-time confocal microscopy with advanced image analysis we were able to track genes within the three-dimensional (3D) space of the nuclear volume of live yeast cells. Because active *GAL* genes have previously been shown to appear closer to the nuclear periphery in fixed cells⁴, we adopted this *GAL* system as a model to explore both the dynamics and the molecular basis of the observed phenomenon. One array of repeated *Tet* operator (*TetO*) was therefore inserted downstream of the *GAL1* gene in a strain expressing the nuclear pore protein Nup49 fused to green fluorescent protein (GFP) (Fig. 1a). This array was revealed *in vivo* by expression of the *Tet* repressor protein coupled to GFP⁸ (Fig. 1a) and subjected to automatic 3D detection and localization over time with correction for Z-detection artefacts (Methods and Supplementary Fig. 1). Visual inspection of the trajectories of *GAL* genes over time revealed a

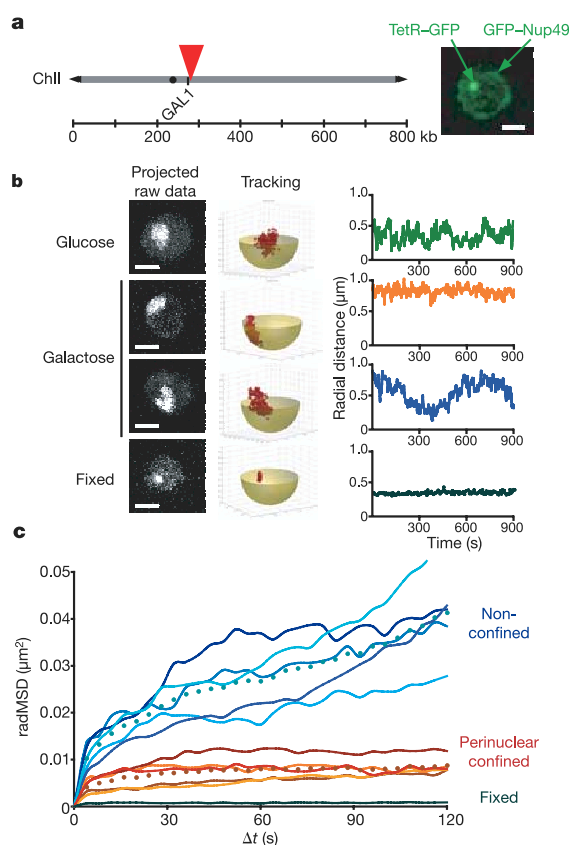


Figure 1 | *In vivo* dynamic analysis of movements of *GAL* genes in three dimensions. **a**, The *GAL* genes were tagged with TetO repeats (red arrowhead). This array labelled by TetR–GFP and the NE labelled with GFP–Nup49 were revealed simultaneously with a Nipkow-disk confocal microscope. kb, kilobases. Scale bar, 1 μ m. **b**, Z and time projection of the whole 3D raw data sequence (left), 3D plot of tracking sequence (centre), and distance between the centroid of the nucleus and the *GAL* genes plotted as a function of time (right) are shown for representative cells (strain yGC105). The entire set of tracking sequences is shown in Supplementary Fig. 2. Scale bar, 1 μ m. **c**, Individual radMSD (Supplementary Fig. 3) computed for each tracking sequence of *GAL* genes in galactose growth condition. The average for each indicated population is plotted as a dotted line.

¹Unité de Biologie Cellulaire du Noyau, ²Unité d'Analyse d'Images Quantitative, and ³Département de Biologie Cellulaire et Infection, Institut Pasteur, 25 rue du Dr Roux, 75724 Paris cedex 15, France. ⁴Biochemie-Zentrum der Universität Heidelberg (BZH), Im Neuenheimer Feld 328, D-69120 Heidelberg, Germany. ⁵Laboratoire de Physique Théorique de la Matière Condensée, 4 place Jussieu, 75252 Paris cedex 05, France. ⁶Institut Pasteur Korea, 39-1, Hawolgok-dong, Sungbuk-gu, Seoul 136-791, Korea. †Present addresses: Institut Pasteur Korea, 39-1, Hawolgok-dong, Sungbuk-gu, Seoul 136-791, Korea (A.G.); Centro de Investigación Príncipe Felipe, Avda Saler 16, 46013 Valencia, Spain (S.R.-N.). *These authors contributed equally to this work.

consistent and marked difference in the dynamic mobility between the repressed state (glucose growth condition) and the actively transcribed state (galactose growth condition, Supplementary Movies). Under glucose repression the tagged locus explored about one-third of the nuclear volume and was often found in the centre of the nucleus (Supplementary movie 1). By contrast, tracks recorded for *GAL* loci under galactose activation often had an exclusive perinuclear localization (Supplementary movie 2). The discrete trajectories of this type of movement usually followed along the nuclear envelope (NE), seemingly being barred from moving back into the nuclear interior. The dynamic motility of a gene can therefore become confined on activation. The type of tethering observed here is not static, because a spatially constrained movement continues along the NE. Rather, our data imply an activation-dependent, dynamic link between the transcribed genes and the NE, permitting a two-dimensional sliding movement underlying the envelope.

When tracking a larger number of cells over time we found that the dynamic change in the movement of activated *GAL* genes is not uniform. Although peripheral confinement was observed in half of the sampled cells, the dynamic motility in the remaining population turned out to be similar to that observed in glucose grown cells (Fig. 1b, and Supplementary Fig. 2). The mean squared change in radial distance (radMSD; Methods and Supplementary Fig. 3a)

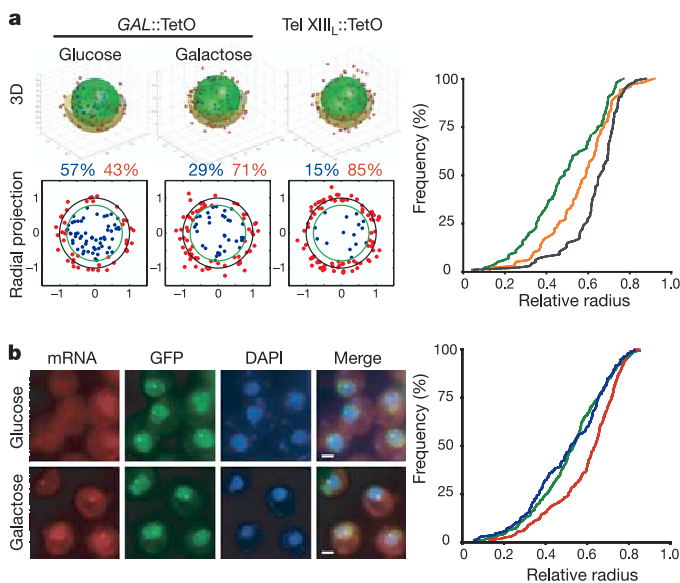


Figure 2 | Localization and expression of *GAL* genes on repression or activation. **a**, After *Z*-stack acquisitions, dedicated software was used to localize throughout the nuclear volume the labelled sub-telomere *Tel XIII_L* (strain *yGC77*) and the *GAL* genes (strain *yGC75*) in glucose-containing or galactose-containing medium in 100 wild-type cells. Left: positions of the tagged loci plotted in both 3D (top) and radial projections (bottom) (see Methods and Supplementary Fig. 1). The nucleus was divided into two equal volumes and the proportion of loci found in each volume is indicated. Right: cumulative distribution functions of the position of the *GAL* locus ($n = 100$; see Methods). Green, *GAL* in glucose-containing medium; orange, *GAL* in galactose-containing medium; black, sub-telomere *Tel XIII_L*. **b**, left: RNA-FISH on wild-type strain (*yGC157*) containing a galactose-dependent *lacZ* gene and the *TetO* array inserted at the *GAL* locus. *lacZ* mRNA (red), *TetR*-GFP and GFP-Nup49 (green) and DNA; DAPI, 4,6-diamidino-2-phenylindole) are shown. Scale bar, 2 μm . Right: cumulative distribution function of *GAL* locus position in glucose ($n = 385$), in galactose when mRNA is not detectable ($n = 178$) and in galactose when mRNA is visible ($n = 360$) are plotted. Pairwise comparisons of these distributions were computed with Kolmogorov-Smirnov tests: galactose with mRNA (red) versus galactose without mRNA (blue), $P = 8.75 \times 10^{-7}$; glucose (green) versus galactose without mRNA, $P = 0.2771$; glucose versus galactose with mRNA, $P = 1.23 \times 10^{-14}$.

plotted as a function of the time interval shows that the radial constraint of the movement does not occur in all cells under activating conditions (Fig. 1c).

To rule out the possibility of a detection artefact or bias inherent in the small sample analysis of dynamic studies, we performed static analyses permitting the statistical investigation of large numbers of cells. To verify the validity of our static approach we compared the extent of galactose-activation-dependent recruitment to the periphery with the previously reported perinuclear positioning of telomeres⁹. As expected, the left end of chromosome XIII was found in the peripheral volume in 85% of the analysed cells (Fig. 2a). Galactose-activated genes were found at the periphery in 71% of the nuclei, whereas repressed genes were evenly distributed throughout the nuclear volume, with only 43% of the loci at the periphery (Fig. 2a). Furthermore, the galactose-dependent recruitment seemed to be independent of the induction time (Supplementary Fig. 4). Taken together, these findings indicate that the activation-dependent recruitment of *GAL* genes might be transient and/or more labile than telomere anchoring.

The apparent inconsistency in the dynamic positioning of *GAL* genes within the same activated population of cells could imply one or both of the following: that genes spend a significant time not being transcribed even though they have been activated (as postulated previously¹⁰) or that only the peripheral loci are expressed. To address these assumptions directly, we performed RNA-fluorescence *in situ* hybridization (FISH) analyses with a probe specific to one single galactose-dependent construct inserted at the *GAL* locus. This experiment allowed us to observe that, on activation, the galactose-dependent transcripts are detected in only two-thirds of the cells (Fig. 2b). Furthermore, the transcribed genes are preferentially found in peripheral positions, whereas loci without detectable mRNA are randomly distributed, which is similar to results with cells grown in glucose-containing medium (Fig. 2b). Taken together, these results demonstrate that the transcriptional state is directly correlated with the position within the nucleus. Apparently, *GAL* genes are preferentially transcribed while their motility is being confined to the NE.

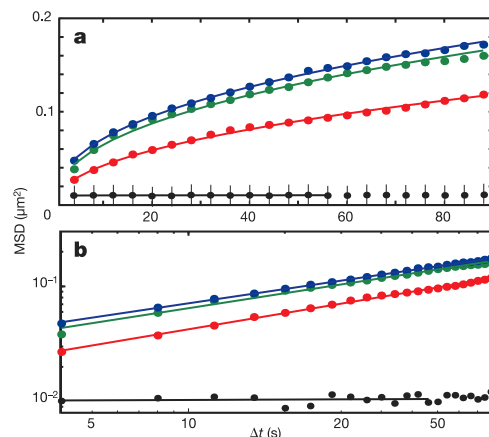


Figure 3 | Mean-squared-displacement analysis of movements of *GAL* genes. **a**, The MSDs (Supplementary Fig. 3) of the *GAL* genes averaged from ten cells grown in glucose (green), five cells grown in galactose for which the *GAL* genes were non-peripheral (blue), five cells grown in galactose for which the *GAL* genes stayed at the periphery (red), and one cell fixed with formaldehyde (black) are plotted in the same graph (strain *yGC105*). Fitted curves are computed for $\Delta t \leq 90$ s. The equations of the curve are as follows: glucose, $y = 0.024x^{0.43}$; non-confined galactose, $y = 0.027x^{0.41}$; perinuclear-confined galactose, $y = 0.014x^{0.47}$; fixed, $y = 0.01x^{0.01}$. **b**, The same set of data plotted with log-log axes. The entire 900-s sequence was used for the calculation but only Δt values from 0 to 90 s are shown.

To characterize the motility of *GAL* genes quantitatively and to enable a better comparison of active and inactive states, the mean squared displacements (MSDs; Methods and Supplementary Fig. 3b) were computed for loci in a repressed state, for loci in an activated state that appeared 'perinuclearly confined', and for 'non-confined' activated loci (Fig. 3). Previous studies have described the dynamics of genetic loci as confined random walks showing a free diffusion motion within the region of confinement¹. In this case, the expected MSD increases linearly with Δt at small time scales (namely $\langle \Delta d^2 \rangle = c(\Delta t)$ with a coefficient of diffusion $D = c/6$) and reaches a plateau at longer times¹¹. By contrast, our experimental data show a markedly different behaviour, with MSD curves at small time scales (less than 90 s) being well fitted by a power-law (namely $\langle \Delta d^2 \rangle = c(\Delta t)^\alpha$) with $\alpha \approx 0.4$, indicating sub-diffusion^{12,13} (Fig. 3). This sub-diffusion movement is observed in all three classes, showing that it depends neither on the transcriptional state nor on the perinuclear position of the *GAL* genes. The difference in motility between the two galactose classes is mostly reflected by a change of the prefactor (c). It decreases to roughly two-thirds for *GAL* genes classified as peripheral, which is consistent with the motion's being restricted to an area along the NE (two-dimensional) instead of a portion of the nuclear volume (3D). In consequence, our data show that both active and inactive *GAL* genes are subject to constrained movement, which cannot be described as a 'confined random walk'. Moreover, spatial repositioning did not at all affect the motility rate of the activated gene. Rather, the active gene sustained its sub-diffusive motility rate in a two-dimensional plane unabated by the presumed perinuclear tether.

The observed repositioning and dynamic confinement of *GAL* loci are clearly linked with transcriptional activation. Activation of *GAL* genes is mediated by the SAGA histone acetyltransferase complex^{14–16}. The Sus1 protein was found as a SAGA member interacting directly with the Sac3–Thp1–Cdc31 mRNA export complex, which is

bound to the nuclear pore complex (NPC) through Nup1 (refs 17–19). Furthermore, Sus1 is required for full *GAL1* gene expression and is physically present at the *GAL1–GAL10* promoter after transcriptional activation¹⁹. To study the effect of those interactions on the positioning of *GAL* genes, we analysed the 3D localization of *GAL* loci in *sac3Δ* and *sus1Δ* mutant strains. We found the galactose-dependent repositioning to be diminished in both mutants (Fig. 4a, b, and Supplementary Fig. 5). The specificity of this observation was corroborated by deletion of the SAGA member *ADA2*, which impaired activation-dependent recruitment, as did the deletion of *NUPI1*, which is consistent with its role in Sac3 localization¹⁸ (Fig. 4a, b, and Supplementary Fig. 5). By contrast, deleting nucleoporins *NUP2* and *NUP53* or the SAGA histone acetyltransferase *GCN5* had no effect (Fig. 4a, b, Supplementary Fig. 5, and data not shown). In addition, Mlp1 or Nup60, components otherwise involved in mRNA retention²⁰, have no direct function in the activation-dependent confinement of *GAL* genes (Supplementary Figs 5 and 6).

Activation-dependent changes in *GAL* positioning are not linked to *GAL1* mRNA transcription levels, which remain unaffected in *ada2Δ* and *nup1Δ* cells, and show only a modest decrease in *sac3Δ* cells (Fig. 4c). Moreover, by employing RNA-FISH we can show that the transcriptional activity of the *GAL* locus continues in *sus1Δ* and *sac3Δ* mutants unabated by the clearly intranuclear positioning of the active *GAL* loci (Supplementary Fig. 7). It indicates that although transcriptional activation is essential for the dynamic link to form, it is not sufficient because mRNA transcription alone does not mediate perinuclear confinement. Considering the direct biochemical interaction of the Sac3–Thp1–Cdc31 complex with both the SAGA complex (through Sus1) and the NPC (through Nup1), our data strongly support the formation of a direct and dynamic link between the activated gene and the NPC.

Taken together, the data presented here indicate that dynamic motility of genes within the nuclear space constitutes a determinant of regulation. Transcriptional factors responsible for gene activation concomitantly 'gate' genes by constraining the 3D motility of activated loci to defined nuclear positions. The resulting link of mRNA transcription and NPC export sites described here is likely to help the preferential processing and export of transcripts. The existence of intranuclear *GAL1* transcription sites in wild-type cells (Fig. 2b) indicates that *GAL* genes are first activated and then 'gated'. However, the reverse may be true for other loci, where the perinuclear position could dictate expression.

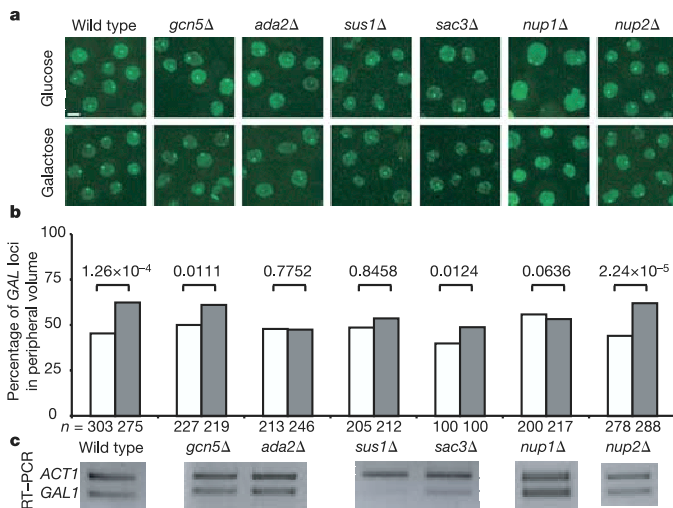


Figure 4 | Localization of *GAL* genes in SAGA and NPC mutants. **a**, *In vivo* 3D localizations of labelled *GAL* genes were performed for wild-type, *GCN5*-, *ADA2*-, *SUS1*-, *SAC3*-, *NUPI1*- and *NUP2*-deleted cells (strains yGC105, yGC197, yGC196, yGC204, yGC205, yGC198 and yGC193, respectively). For each mutant, examples of 3D raw data are shown Z-projected in both glucose and galactose. Scale bar, 2 μ m. **b**, Bar graph indicating the proportion of *GAL* loci found in the peripheral volume (as defined in Supplementary Fig. 1). Pairwise comparisons of the distributions of R3Dp (see Methods) computed for each strain and growth condition were performed with Kolmogorov–Smirnov tests. The *P* value is indicated above the bracket for each test; *n* is the number of cells analysed. Open bars, glucose; filled bars, galactose. **c**, Level of *GAL1* transcripts in the galactose growth condition analysed in each mutant by RT–PCR followed by agarose-gel electrophoresis. *ACT1* transcripts are also included as a control.

METHODS

Microscopy. Live microscopy was performed with a Perkin-Elmer UltraView RS Nipkow-disk confocal system controlled with PE-viewer software (version 1.0.0.9) featuring a Zeiss 100 \times objective (Plan Apo, 1.4 NA, oil immersion). The pixel size was 65.8 nm. For 3D static analysis, Z-stacks of 51 images with a 200-nm Z-step were used. The exposure time was 200 ms for GFP. For 3D dynamic analysis, 25-image Z-stacks with a Z-step of 250 nm and an acquisition time of 150 ms were taken every 4 s for 15 min (226 time points; 5,650 images).

RNA fluorescent *in situ* hybridization was performed as described²⁰.

Image analysis. Detection and tracking of GFP-tagged chromosomal loci and the NE in each Z-stack series were performed automatically with a dedicated software described in Supplementary Methods. After processing, the SPB labelled with Spc29–GFP was used as an internal reference to correct the Z-detection artefact (Supplementary Fig. 1a, b). Finally, the position in the nuclear volume of the detected locus is given by the relative 3D position (R3Dp), which is the ratio of (corrected distance between the centroid of the nucleus and the labelled locus) to (corrected radius). The nuclear space was divided into two concentric zones of equal volume (Supplementary Fig. 1c) and in each experiment the percentages of loci distributed between these two volumes computed over the cell sample of R3Dp are given. The cumulative distribution function (CDF), 3D graph and radial projection were plotted with Matlab software, version 7.0.4. Kolmogorov–Smirnov tests were performed and significance was determined with 95% confidence limits. Time-lapse experiments were analysed by computing the radMSD (Supplementary Fig. 3a) and the MSD (Supplementary Fig. 3b) with Matlab software, version 7.0.4.

Plasmids, strains, growth conditions, RT–PCR protocol and details of

quantitative image analysis and brownian motion analysis are described in Supplementary Methods.

Received 27 January; accepted 24 March 2006.

- Spector, D. L. The dynamics of chromosome organization and gene regulation. *Annu. Rev. Biochem.* **72**, 573–608 (2003).
- Andrulis, E. D., Neiman, A. M., Zappulla, D. C. & Sternglanz, R. Perinuclear localization of chromatin facilitates transcriptional silencing. *Nature* **394**, 592–595 (1998).
- Casolari, J. M., Brown, C. R., Drubin, D. A., Rando, O. J. & Silver, P. A. Developmentally induced changes in transcriptional program alter spatial organization across chromosomes. *Genes Dev.* **19**, 1188–1198 (2005).
- Casolari, J. M. *et al.* Genome-wide localization of the nuclear transport machinery couples transcriptional status and nuclear organization. *Cell* **117**, 427–439 (2004).
- Brickner, J. H. & Walter, P. Gene recruitment of the activated INO1 locus to the nuclear membrane. *PLoS Biol.* **2**, e342 (2004).
- Menon, B. B. *et al.* Reverse recruitment: the Nup84 nuclear pore subcomplex mediates Rap1/Gcr1/Gcr2 transcriptional activation. *Proc. Natl Acad. Sci. USA* **102**, 5749–5754 (2005).
- Blobel, G. Gene gating: a hypothesis. *Proc. Natl Acad. Sci. USA* **82**, 8527–8529 (1985).
- Michaelis, C., Ciosk, R. & Nasmyth, K. Cohesins: chromosomal proteins that prevent premature separation of sister chromatids. *Cell* **91**, 35–45 (1997).
- Gotta, M. *et al.* The clustering of telomeres and colocalization with Rap1, Sir3, and Sir4 proteins in wild-type *Saccharomyces cerevisiae*. *J. Cell Biol.* **134**, 1349–1363 (1996).
- Kimura, H., Sugaya, K. & Cook, P. R. The transcription cycle of RNA polymerase II in living cells. *J. Cell Biol.* **159**, 777–782 (2002).
- Vazquez, J., Belmont, A. S. & Sedat, J. W. Multiple regimes of constrained chromosome motion are regulated in the interphase *Drosophila* nucleus. *Curr. Biol.* **11**, 1227–1239 (2001).
- Havlin, S. & Ben-Avraham, D. Diffusion in disordered media. *Adv. Phys.* **51**, 187–292 (2002).
- Bouchaud, J. P. & Georges, A. Anomalous diffusion in disordered media: statistical mechanics, models and physical applications. *Phys. Rep.* **195**, 127–293 (1990).
- Huisinga, K. L. & Pugh, B. F. A genome-wide housekeeping role for TFIID and a highly regulated stress-related role for SAGA in *Saccharomyces cerevisiae*. *Mol. Cell* **13**, 573–585 (2004).
- Bhaumik, S. R. & Green, M. R. SAGA is an essential *in vivo* target of the yeast acidic activator Gal4p. *Genes Dev.* **15**, 1935–1945 (2001).
- Larschan, E. & Winston, F. The *S. cerevisiae* SAGA complex functions *in vivo* as a coactivator for transcriptional activation by Gal4. *Genes Dev.* **15**, 1946–1956 (2001).
- Fischer, T. *et al.* Yeast centrin Cdc31 is linked to the nuclear mRNA export machinery. *Nature Cell Biol.* **6**, 840–848 (2004).
- Fischer, T. *et al.* The mRNA export machinery requires the novel Sac3p-Thp1p complex to dock at the nucleoplasmic entrance of the nuclear pores. *EMBO J.* **21**, 5843–5852 (2002).
- Rodríguez-Navarro, S. *et al.* Sus1, a functional component of the SAGA histone acetylase complex and the nuclear pore-associated mRNA export machinery. *Cell* **116**, 75–86 (2004).
- Galy, V. *et al.* Nuclear retention of unspliced mRNAs in yeast is mediated by perinuclear Mlp1. *Cell* **116**, 63–73 (2004).

Supplementary Information is linked to the online version of the paper at www.nature.com/nature.

Acknowledgements We thank D. Fagegaltier, E. Fabre, P. Therizol, B. Zhang, T. Fischer and all the members of the Nehrbass group for critical discussions, and A. Taddei and S. Gasser for sharing unpublished results. We thank the 'Plateforme d'imagerie dynamique' of the Pasteur Institute for providing access to the microscopy facilities. This work was supported by an ACI-BCMS grant. G.G.C. and A.G. were recipients of fellowships of the Ministère Français délégué à la Recherche et aux Nouvelles Technologies.

Author Contributions E.C.H. and U.N. conceived the project. G.G.C. did the experiments. S.R.-N. did the RT-PCR experiment. G.G.C. and O.G. conceived the image analysis protocols. A.G. and J.-C.O.-M. conceived the image analysis algorithms in collaboration with G.G.C. and O.G. A.G. implemented the image analysis algorithms. G.G.C. did the image processing and analysis. G.G.C. and C.Z. computed the MSD. G.G.C., O.G., C.Z., H.B. and A.L. interpreted the image analysis results. G.G.C., S.R.-N. and F.F.-F. provided the yeast strains and plasmid constructs. U.N. wrote the paper. F.F.-F. supervised G.G.C. J.-C.O.-M. supervised A.G. J.-C.O.-M., E.C.H. and U.N. are head of the laboratories participating in this work.

Author Information Reprints and permissions information is available at npg.nature.com/reprintsandpermissions. The authors declare no competing financial interests. Correspondence and requests for materials should be addressed to U.N. (nehrbass@pasteur.fr) or E.C.H. (cg5@ix.urz.uni-heidelberg.de). Any requests for imaging software should be addressed to J.-C.O.-M. (jcolivo@pasteur.fr).